CHEMISTRY

Surface-modified, dye-sensitized niobate nanosheets enabling an efficient solar-driven Z-scheme for overall water splitting

Shunta Nishioka[1]†, Koya Hojo[1]†, Langqiu Xiao[2], Tianyue Gao[2], Yugo Miseki[3], Shuhei Yasuda[4], Toshiyuki Yokoi[4], Kazuhiro Sayama[3], Thomas E. Mallouk[2,5]*, Kazuhiko Maeda[1]*

While dye-sensitized metal oxides are good candidates as H_2 evolution photocatalysts for solar-driven Z-scheme water splitting, their solar-to-hydrogen (STH) energy conversion efficiencies remain low because of uncontrolled charge recombination reactions. Here, we show that modification of Ru dye–sensitized, Pt-intercalated $HCa_2Nb_3O_{10}$ nanosheets (Ru/Pt/$HCa_2Nb_3O_{10}$) with both amorphous Al_2O_3 and poly(styrenesulfonate) (PSS) improves the STH efficiency of Z-scheme overall water splitting by a factor of ~100, when the nanosheets are used in combination with a WO_3-based O_2 evolution photocatalyst and an I_3^-/I^- redox mediator, relative to an analogous system that uses unmodified Ru/Pt/$HCa_2Nb_3O_{10}$. By using the optimized photocatalyst, PSS/Ru/Al_2O_3/Pt/$HCa_2Nb_3O_{10}$, a maximum STH of 0.12% and an apparent quantum yield of 4.1% at 420 nm were obtained, by far the highest among dye-sensitized water splitting systems and comparable to conventional semiconductor-based suspended particulate photocatalyst systems.

INTRODUCTION

The development of artificial photosynthetic assemblies that can use the broad wavelength range of visible light and are operable under weak-intensity conditions (e.g., sunlight irradiation) is a long-standing challenge in energy research. Semiconductor photocatalysis is one of the most promising options for realizing clean H_2 production from renewable resources on a large scale (*1*, *2*). For any artificial photosynthetic scheme in which the standard Gibbs free energy change is positive, it is particularly important to suppress the rate of backward reactions including back electron transfer (*1*, *3*–*6*). In Z-scheme overall water splitting using two different photocatalysts in the presence of a shuttle redox mediator, for example, photogenerated electrons in the H_2-evolving photocatalyst must be consumed by reduction of H_2O (or protons) to H_2 while minimizing the reduction of more reducible electron-accepting species, which must be reduced by the O_2-evolving photocatalyst (*4*).

Dye-sensitized wide-bandgap semiconductors with proper modifications are capable of catalyzing water reduction to H_2 under visible light even in the presence of reversible electron donors such as I^- (*7*, *8*). Hence, they are potential candidates as H_2 evolution photocatalysts for Z-scheme overall water splitting (*9*–*12*). Modification of a Ru dye–loaded layered niobate with poly(styrenesulfonate) (PSS) has previously been shown to improve the efficiency of dye-sensitized H_2 evolution from aqueous KI solutions, while the use of undecylphosphonic acid or methylphosphonic acid, which do not form good surface monolayers, did not (*8*). In that case, the PSS layer on the niobate could selectively exclude I_3^-, the oxidation product of I^-, from the semiconductor/solution interface, thereby suppressing the back electron transfer reaction between electrons in the conduction band of the niobate and I_3^-. Recently, it has been shown that restacked niobate nanosheets sensitized by a Ru(II) tris-diimine complex also act as good building blocks for the construction of Z-scheme overall water splitting systems, which outperform the parent layered analogs (*10*). An attractive feature of the oxide nanosheet is its high specific surface area, which enables it to accommodate more dye molecules on its surface, as compared to the parent lamellar solids (*10*, *13*, *14*). However, the high surface area of oxide nanosheets may act negatively by providing more exposed surface for the back electron transfer reaction, thereby lowering the overall efficiency.

In this work, we show that Ru dye–sensitized niobate nanosheets, further modified with Al_2O_3 and PSS layers, work as an efficient H_2 evolution photocatalyst in Z-scheme overall water splitting in combination with a PtO_x/H-Cs-WO_3 oxygen-evolving photocatalyst and an I_3^-/I^- redox shuttle even under the weak intensity of simulated sunlight. As expected, our experiments showed that the undesirable back electron transfer reactions occur very efficiently on the Ru dye–sensitized nanosheets, thereby contributing to low solar-to-hydrogen (STH) energy conversion efficiency for overall water splitting. On the other hand, dual modification by Al_2O_3 and PSS enables nearly two orders of magnitude improvement in STH efficiency under optimized conditions.

RESULTS

Half-cell H_2 evolution reactions

Following the method described in our previous report (*10*, *15*), calcium niobate nanosheets intercalated with Pt nanoclusters were synthesized, and modification of the as-prepared Pt/$HCa_2Nb_3O_{10}$ with an amorphous Al_2O_3 overlayer and $[Ru(dmb)_2(4,4'\text{-}(PO_3H_2)_2bpy)]^{2+}$ (dmb = 4,4′-dimethyl-2,2′-bipyridine, bpy = 2,2′-bipyridine), abbreviated as **Ru**, was conducted. Loading PSS onto the nanosheet

[1]Department of Chemistry, School of Science, Tokyo Institute of Technology, 2-12-1-NE-2 Ookayama, Meguro-ku, Tokyo 152-8550, Japan. [2]Department of Chemistry, University of Pennsylvania, 231 S. 34th Street Philadelphia, PA 19104, USA. [3]Global Zero Emission Research Center (GZR), National Institute of Advanced Industrial Science and Technology (AIST), West, 16-1, Onogawa, Tsukuba, Ibaraki 305-8569, Japan. [4]Nanospace Catalysis Unit, Institute of Innovative Research, Tokyo Institute of Technology, Yokohama 226-8503, Japan. [5]International Center for Materials Nanoarchitectonics (WPI-MANA), National Institute for Materials Science (NIMS), Tsukuba, Ibaraki 305-0044, Japan.
*Corresponding author. Email: maedak@chem.titech.ac.jp (K.M.); mallouk@sas.upenn.edu (T.E.M.)
†These authors contributed equally to this work.

materials was performed at room temperature by dispersing the dye-adsorbed niobate nanosheets in a sodium polystyrene sulfonate aqueous solution at pH 2 for 1 hour (*8*). No significant change in the morphology of the Pt/$HCa_2Nb_3O_{10}$ nanosheets was seen before and after the PSS modification step (fig. S1). Energy-dispersive x-ray spectroscopy was also carried out to visualize the distribution of PSS on the nanosheets, but did not give meaningful results. This was because of the low concentration of the loaded PSS, as confirmed by x-ray photoelectron spectroscopy (XPS) measurements. As shown in fig. S2, a clear S 2p photoelectron signal at 168.0 eV, assignable to PSS (*16*), was observed, but with very low concentration of PSS; the surface atomic ratio of S/Nb in the PSS/Pt/$HCa_2Nb_3O_{10}$ was about 0.04. It should be noted that the ^{1}MLCT absorption band of the adsorbed **Ru** at around 460 nm was maintained even after PSS modification (fig. S3).

First, half-cell H_2 evolution reactions were conducted using **Ru**/Pt/$HCa_2Nb_3O_{10}$ with and without postmodification under two different light intensity conditions using a 300-W xenon lamp. A schematic illustration of the energy diagram of the **Ru**-sensitized Pt/$HCa_2Nb_3O_{10}$ nanosheets for H_2 evolution is shown in Fig. 1. The reaction consists of reduction of H^+ into H_2 on the intercalated Pt in the nanosheet photocatalyst and oxidation of I^- into I_3^- by one-electron oxidized **Ru** as follows

$$2H^+ + 2e^- \rightarrow H_2(\text{reduction of } H^+ \text{ into } H_2) \quad (1)$$

$$3I^- + 2h^+ \rightarrow I_3^-(\text{oxidation of } I^- \text{ into } I_3^-) \quad (2)$$

As shown in Fig. 2A, the **Ru**/Pt/$HCa_2Nb_3O_{10}$ produced H_2 from aqueous NaI solution under high-intensity visible light (80 mW cm^{-2}, $\lambda > 400$ nm), but the H_2 evolution rate was slowed down after only 1 hour of irradiation. This can be explained by the increasing predominance of the back reaction involving the oxidized donor (I_3^-) and the injected electrons in the Pt/$HCa_2Nb_3O_{10}$ nanosheets (Eq. 3), which is thermodynamically more favorable than the forward reaction of proton reduction (Eq. 1) (*7*, *8*)

$$I_3^- + 2e^- \rightarrow 3I^-(\text{reduction of } I_3^- \text{ into } I^-) \quad (3)$$

Al_2O_3 modification has been reported to suppress back electron transfer reaction from the conduction band of a metal oxide to the oxidized form of the Ru dye in Ru dye–sensitized metal oxide systems (*11*, *17*). In the present **Ru**/Pt/$HCa_2Nb_3O_{10}$ system, Al_2O_3 modification did not measurably improve the H_2 evolution activity. Modification of the **Ru**/Pt/$HCa_2Nb_3O_{10}$ with PSS also had no measurable impact on the H_2 evolution activity under these conditions. These results imply that the negative impact of the backward reaction on the **Ru**/Pt/$HCa_2Nb_3O_{10}$ (Eq. 3) is significant under high-intensity irradiation conditions.

On the other hand, when the reactions were conducted under lower-intensity visible light (8.0 mW cm^{-2}, $\lambda > 400$ nm), a clear enhancement effect by PSS modification appeared (Fig. 2B). In contrast to the high–light intensity condition, the concentration of I_3^- produced should be lower under low-intensity irradiation. Under these conditions, the injected electrons in the conduction band of the nanosheets have a higher probability of escaping from recombination with I_3^- and reacting with protons at the intercalated Pt. Thus, the positive effect of PSS modification on H_2 evolution activity becomes apparent only when the concentration of I_3^- in the reaction system is sufficiently low. It is also noted that the Al_2O_3 modification slightly improved the H_2 evolution activity under low–light intensity conditions, suggesting that the primary role of the Al_2O_3 modifier is to suppress the back electron transfer reaction from the oxide to the adsorbed dye, as noted above. In other words, when I_3^- is present even at low concentration, back electron transfer to I_3^- will occur more readily than reverse electron transfer to the oxidized Ru dye.

Effect of dual modification with Al_2O_3 and PSS

On the basis of these results, we can expect that the promotional effect of chemical modifiers on H_2 evolution by the **Ru**/Pt/$HCa_2Nb_3O_{10}$ photocatalyst will be maximized if the concentration of I_3^- in the reaction solution is minimized. This situation can be realized in the presence of an O_2 evolution photocatalyst, which can efficiently reduce I_3^- into I^- and oxidize water into O_2. With this idea in mind, Z-scheme overall water splitting systems were constructed using **Ru**/Pt/$HCa_2Nb_3O_{10}$ with different modifications in the presence of

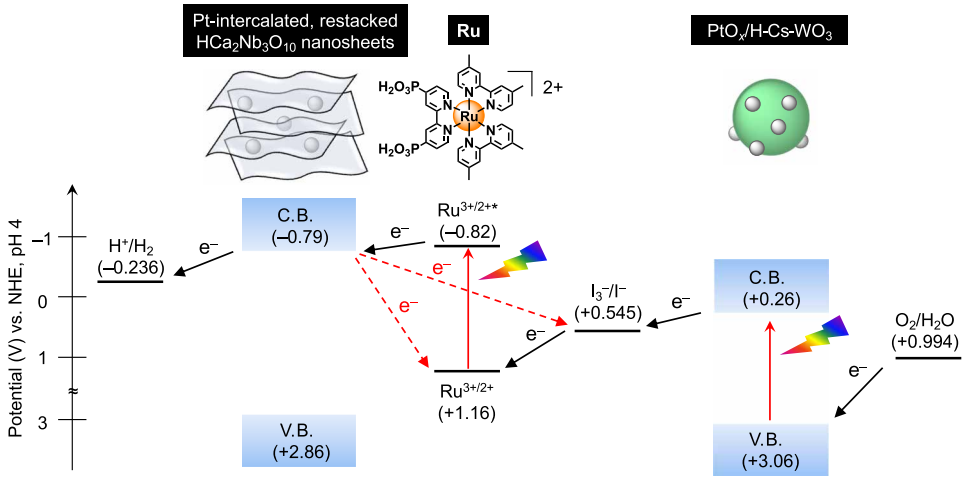

Fig. 1. Electron transfer mechanism. Schematic electron transfer mechanism and energy level diagram of the **Ru**/Pt/$HCa_2Nb_3O_{10}$ nanosheets for H_2 evolution and PtO_x/H-Cs-WO_3 for O_2 evolution. C.B., conduction band; V.B., valence band.

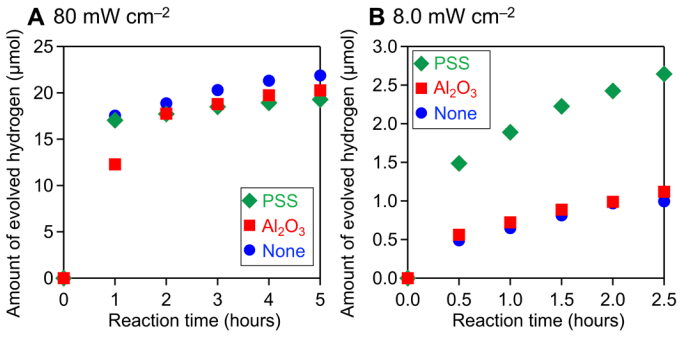

Fig. 2. Half-cell H_2 evolution reactions. Time courses of H_2 evolution from an aqueous NaI solution over **Ru**/Pt/$HCa_2Nb_3O_{10}$ nanosheets with different modifications. Reaction conditions: catalyst, 20 mg; solution, aqueous NaI (10 mM, 100 ml, pH 3.8 to 4.0); light source, xenon lamp (300 W) fitted with CM-1 cold mirror and L42 cutoff filter (λ > 400 nm). Irradiation area, 44 cm^2. (**A** and **B**) Data taken under higher-intensity (80 mW cm^{-2}) and lower-intensity (8.0 mW cm^{-2}) irradiation, respectively. Experimental error in the H_2 amount was ~20%.

a PtO_x/H-Cs-WO_3 photocatalyst, which has been reported to work efficiently even at low concentration of I_3^- and to produce O_2 (*18*).

Table 1 lists the results of Z-scheme overall water splitting reactions, which were conducted under high-intensity visible light (80 mW cm^{-2}, λ > 400 nm). Full time course data are shown in fig. S4. When **Ru**/Pt/$HCa_2Nb_3O_{10}$ was used, a larger amount of H_2 (57.7 μmol) as well as nearly stoichiometric O_2 was produced in the Z-scheme reaction (entry 1), as compared to that in the half-cell H_2 evolution (21.9 μmol; Fig. 2A). This confirms that back electron transfer to I_3^- can be suppressed in the H_2 evolution photocatalyst, owing to the fact that the O_2 evolution photocatalyst efficiently consumes I_3^- ions. As expected from the results of half reaction at low light intensity (Fig. 2B), PSS modification enhanced the overall water splitting activity (entry 2). While the Al_2O_3 modification had little impact on the half-cell H_2 evolution rate even under low light intensity (Fig. 2B), it increased the Z-scheme activity by a factor of 3 (entry 3). These results can also be explained in terms of the I_3^- concentration. When the local concentration of I_3^- around the H_2 evolution photocatalyst is high (e.g., in the half reaction), electron transfer from $HCa_2Nb_3O_{10}$ to I_3^- is efficient. Under this condition, the Al_2O_3 modification only slightly influences the yield of hydrogen, even if it has a positive effect on suppressing back electron transfer to the oxidized Ru dye. At low concentration of I_3^-, on the other hand, the back electron transfer to I_3^- is less efficient, and so back electron transfer to the oxidized Ru dye becomes more kinetically competitive with hydrogen evolution. This qualitatively implies the positive effect of Al_2O_3 modification.

Thus, the two modifiers were shown to behave differently, depending on the local concentration of I_3^- around, or adsorption of I_3^- onto, the surface of the H_2 evolution photocatalyst. Both modifiers provide a positive kinetic effect on the activity under Z-scheme water splitting conditions; Al_2O_3 should primarily suppress back electron transfer to the surface-adsorbed oxidized **Ru** complex, whereas PSS should inhibit reduction of I_3^-. Here, we combined both of the modifiers and found that the doubly modified sample was more active than the individually modified analogs (entry 4). In this system, it is reasonable that both back electron transfer reactions are suppressed more effectively, and thus, the injected electrons in $HCa_2Nb_3O_{10}$ can more efficiently react at the intercalated Pt to evolve H_2.

Table 1. Z-scheme overall water splitting under visible light.
Photocatalytic activities of **Ru**-sensitized Pt/$HCa_2Nb_3O_{10}$ nanosheets with different modifications for Z-scheme water splitting with PtO_x/H-Cs-WO_3 under high-intensity visible light (80 mW cm^{-2}, λ > 400 nm).*

Entry	H_2 evolution photocatalyst	Evolved gases† (μmol)	
		H_2	O_2
1	**Ru**/Pt/$HCa_2Nb_3O_{10}$	57.7	26.6
2	PSS/**Ru**/Pt/$HCa_2Nb_3O_{10}$	125.0	56.1
3	**Ru**/Al_2O_3/Pt/$HCa_2Nb_3O_{10}$	174.0	79.3
4	PSS/**Ru**/Al_2O_3/Pt/$HCa_2Nb_3O_{10}$	425.8	200.3

*Reaction conditions: catalyst, modified **Ru**/Pt/$HCa_2Nb_3O_{10}$, 20 mg; PtO_x/H-Cs-WO_3, 50 mg; reactant solution, 5 mM aqueous NaI (100 ml, pH 4); light source, xenon lamp (300 W) with a cold mirror (CM-1) and a cutoff filter (L42). Irradiation area, 44 cm^2. †Total amount after 5-hour irradiation.

To further investigate the effects of Al_2O_3 and PSS modification on the excited charge carrier dynamics, laser flash photolysis/transient absorption measurements were carried out. By observing transient bleaching recovery of the dye without any added reducing agent, one can measure the rate of back electron transfer from the semiconductor to the oxidized Ru complex. Following a laser flash at 532 nm to selectively photoexcite **Ru**, bleaching of the ^{1}MLCT absorption of ground-state **Ru** was observed at 475 nm (fig. S5). As reported previously (*10*), Al_2O_3 modification clearly decelerated the bleaching recovery, indicating that the back electron transfer reaction is suppressed. Although a similar effect was observed with PSS-modified samples, the decrease in the bleaching recovery rate was not as great as with Al_2O_3.

By monitoring the transient absorbance in an aqueous NaI solution, the reactivity of the photocatalyst with iodide ions can be measured. In this case, the bleaching recovery of the ^{1}MLCT absorbance provides information about the rate of electron transfer from I^- to the oxidized dye. Figure 3A shows time-dependent change in the ^{1}MLCT absorption of **Ru** for Al_2O_3 and PSS-modified samples in aqueous NaI solutions. The Al_2O_3 modifier markedly accelerates the bleaching recovery in the presence of I^-, indicating that Al_2O_3 promotes the reaction between the oxidized **Ru** complex and iodide ions. As noted previously (*11*), because Al_2O_3 modification makes the surface ζ-potential positive, anions in the solution can access the surface of the photocatalyst more readily. This implies that triiodide ions are also attracted to the surface of the Al_2O_3-modified photocatalyst. On the contrary, the PSS modifier clearly decelerates the ^{1}MLCT bleaching recovery. The reverse effect of PSS, as compared with Al_2O_3, is understandable because PSS is an anionic polymer. Retardation of the ^{1}MLCT bleaching recovery was observed even with dual modification by Al_2O_3 and PSS. It is, therefore, expected that the PSS modifier inhibits the access of not only I^- but also I_3^- to the photocatalyst surface.

The reactivity of conduction band electrons in the semiconductor with triiodide ion can be followed by measuring the transient absorbance change at 380 nm, where I_3^- absorbs strongly (*8*). To obtain a high signal intensity of I_3^-, this measurement was conducted

in 100 mM aqueous NaI solution where recovery of the ground state of **Ru** is very fast. The time-dependent absorbance changes at 380 nm are shown in Fig. 2B, and the measured lifetimes are tabulated in Table 2. All the profiles could be fitted by double- or triple-exponential functions (Eqs. 4 and 5)

$$f(x) = y_0 + A_1 \exp\left(-\frac{x - x_0}{\tau_1}\right) - A_2 \exp\left(-\frac{x - x_0}{\tau_2}\right) \quad (4)$$

$$f(x) = y_0 + A_1 \exp\left(-\frac{x - x_0}{\tau_1}\right) - A_2 \exp\left(-\frac{x - x_0}{\tau_2}\right) - A_3 \exp\left(-\frac{x - x_0}{\tau_3}\right) \quad (5)$$

In each case, there was an abrupt increase in the ΔO.D. and a subsequent decay, which correspond to an increase and decrease in the triiodide concentration, respectively. Unmodified and Al_2O_3-modified samples had a positive component (τ_1), corresponding to generation of I_3^-, which was one order of magnitude faster than that of the PSS-modified samples, confirming again that the PSS modifier suppresses the reaction of I^- with the surface-bound oxidized **Ru** complex. While the acceleration of this reaction by Al_2O_3 modification was clear in the 475-nm transient (the ^{1}MLCT bleaching recovery; Fig. 3A), the trend was obscured at 380 nm. This is probably because the time window for monitoring the absorption changes of I_3^- was 16 ms, far longer than the τ_1 values (<1 μs). On the other hand, an obvious increase in the ΔO.D. was seen with the Al_2O_3-modified sample, which is consistent with acceleration of the reaction of I^- with the oxidized **Ru** complex by Al_2O_3 modifier.

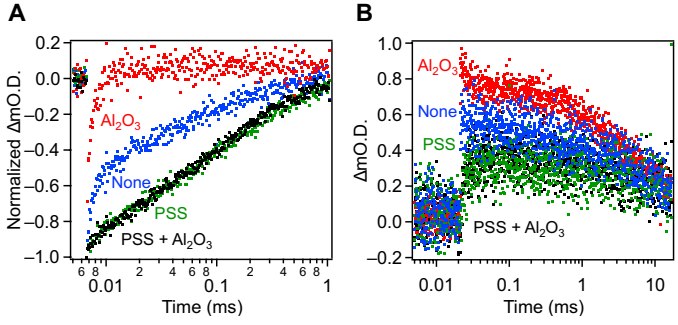

Fig. 3. Transient diffuse reflectance decay. Time-dependent absorbance change in transient diffuse reflectance measurements of **Ru**-sensitized $HCa_2Nb_3O_{10}$ nanosheets with and without surface modification recorded in aqueous NaI solutions (pH 4.0) monitored at (**A**) 475 nm (10 mM NaI) and (**B**) 380 nm (100 mM NaI).

The τ_2 component mainly reflects the recombination reaction, in which conduction band electrons are scavenged by I_3^- (Eq. 3). The millisecond-order absorption decay lifetime of τ_2 is consistent with earlier observations (*8*). Unmodified and Al_2O_3-modified samples had τ_2 values that were similar to each other, indicating that Al_2O_3 does not effectively suppress this recombination reaction. On the contrary, PSS modification resulted in a nearly twofold longer τ_2, indicating clear inhibition of the reduction of I_3^-. It is most likely that suppression of the reactions of both I^- and I_3^- by PSS results from electrostatic repulsion between the anionic polymer and the anions. This effect is also evident with the PSS/Al_2O_3 comodified sample. Another important observation is that there is an additional lifetime component (τ_3) that is needed to fit the decay curve of the Al_2O_3-modified sample. τ_3 is one of the decay components of the I_3^- absorption and is significantly shorter than τ_2. The appearance of a very short lifetime component obviously suggests that there is a very fast decay process involving I_3^- in the Al_2O_3-modified photocatalyst.

From the results of transient absorption spectroscopy, it is apparent that the PSS modifier alone can suppress the reduction of I_3^- (the recombination reaction) in Z-scheme water splitting, but the reaction with I^- (the forward reaction) is also decelerated. PSS modification alone does not suppress back electron transfer from the semiconductor to the oxidized **Ru** complex, a rapid reaction that can compete kinetically with the reduction of I_3^-. Therefore, the full potential of the nanosheet photocatalyst for Z-scheme water splitting is reached only by dual modification with Al_2O_3 and PSS. We note that the retardation of the reaction with I^- by PSS does not significantly affect the photocatalytic activity of the Z-scheme. This is because the reaction of I^- with the oxidized **Ru** complex is always much faster than the photocatalytic reactions, as demonstrated in our previous studies (*11*). A schematic reaction mechanism that we propose is shown in fig. S6.

Solar-driven Z-scheme overall water splitting

The difference in Z-scheme activity among the differently modified nanosheet photocatalysts was found to be much clearer when the Z-scheme reactions were conducted under simulated sunlight. Figure 4 shows STH energy conversion efficiencies recorded under different light intensity conditions using **Ru**/Pt/$HCa_2Nb_3O_{10}$

Table 2. Absorption decay lifetimes. Absorption decay lifetimes of **Ru** adsorbed on $HCa_2Nb_3O_{10}$ nanosheets with different surface modifications.

Entry	H_2 evolution photocatalyst	τ_1 (μs)	τ_2 (μs)	τ_3 (μs)
		%	%	%
1	**Ru**/Pt/$HCa_2Nb_3O_{10}$	0.22 ± 0.07	3200 ± 300	–
		62	38	
2	PSS/**Ru**/Pt/$HCa_2Nb_3O_{10}$	2.6 ± 0.7	7000 ± 3000	–
		60	40	
3	**Ru**/Al_2O_3/Pt/$HCa_2Nb_3O_{10}$	0.26 ± 0.03	3400 ± 100	5 ± 1
		59	30	11
4	PSS/**Ru**/Al_2O_3/Pt/$HCa_2Nb_3O_{10}$	3 ± 1	7000 ± 2000	–
		48	52	

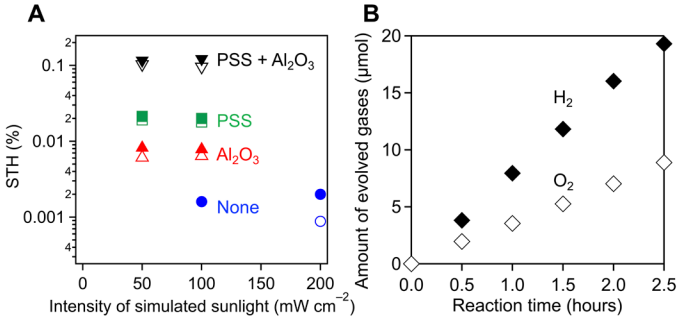

Fig. 4. Solar-driven Z-scheme overall water splitting. (**A**) STH energy conversion efficiencies of **Ru**/Pt/$HCa_2Nb_3O_{10}$ nanosheets with different modifications for Z-scheme water splitting. (**B**) Time courses of H_2 and O_2 evolution from a mixture of PSS/**Ru**/Al_2O_3/Pt/$HCa_2Nb_3O_{10}$ and PtO_x/H-Cs-WO_3 under simulated sunlight (50 mW cm^{-2}). Reaction conditions: catalyst, modified **Ru**/Pt/$HCa_2Nb_3O_{10}$, 20 mg; PtO_x/H-Cs-WO_3, 50 mg; reactant solution, 5 mM aqueous NaI (100 ml, pH 4); light source, solar simulator with an irradiation area of 9 cm^2. Closed and open symbols indicate data based on H_2 and O_2 evolution, respectively.

nanosheets with different modifications. Under 1-Sun conditions (100 mW cm^{-2}), the **Ru**/Pt/$HCa_2Nb_3O_{10}$-based system produced H_2 moderately with little O_2 evolution, and the STH could not be calculated on the basis of the O_2 evolution rate. Both H_2 and O_2 evolution were observable under 2-Sun conditions, giving STHs of 0.0020 and 0.00088% based on each gas evolution rate. Thus, higher light intensity was necessary for the **Ru**/Pt/$HCa_2Nb_3O_{10}$ nanosheets without modification to operate as a Z-scheme overall water splitting system.

On the other hand, the PSS/**Ru**/Pt/$HCa_2Nb_3O_{10}$ nanosheets gave a nearly 10-fold enhancement in STH, as compared to an analogous system without PSS. The system worked even under 0.5-Sun conditions, with almost the same STH value of ~0.02% as that recorded under 1-Sun conditions. The Al_2O_3 modification also provided an enhancement effect similar to PSS, but the effect was less pronounced. This is opposite to the trend observed in Z-scheme experiments under high-intensity visible light, where Al_2O_3 was better than PSS (Table 1). From these results, we postulate that the back electron transfer to I_3^- ions is more efficient than that to the oxidized **Ru** under low light intensity conditions. This idea is consistent with the results of the half-cell H_2 evolution reactions (Fig. 2B).

The largest improvement in STH was seen when the PSS and Al_2O_3 modifications were combined. Nearly two orders of magnitude higher STH (~0.12%) was obtained with the optimally modified nanosheet photocatalyst, relative to **Ru**/Pt/$HCa_2Nb_3O_{10}$. This value is comparable to those reported in typical powder-suspension–type Z-scheme systems [e.g., Ru/$SrTiO_3$:Rh + $BiVO_4$ with $Fe^{3+/2+}$ redox (0.1%) (*19*) and Pt/ZrO_2/TaON + PtO_x/WO_3 with IO_3^-/I^- redox (0.19 ± 0.02%) (*20*)]. The PSS/**Ru**/Al_2O_3/Pt/$HCa_2Nb_3O_{10}$-based system produced stoichiometric H_2 and O_2, as shown in Fig. 3B.

Thus, it is clear that modification with Al_2O_3 (and/or PSS) makes the **Ru**/Pt/$HCa_2Nb_3O_{10}$ nanosheets operable even under light with low intensity. Domen and co-workers (*21*) have reported that GaN:ZnO photocatalysts, modified with an Rh-Cr mixed oxide cocatalyst, required high light intensity for overall water splitting when the rate of electron-hole recombination is significant in the photocatalyst. A report by Osterloh and co-workers (*22*) has shown a similar phenomenon; a Ru/$SrTiO_3$:Rh–$BiVO_4$ composite photocatalyst designed for Z-scheme overall water splitting does not work efficiently under low-intensity visible light because of recombination of minority carriers at the Ru/$SrTiO_3$:Rh–$BiVO_4$ interface. In our system, because the **Ru**/Pt/$HCa_2Nb_3O_{10}$ nanosheets have undesirable back electron transfer pathways that favor charge carrier recombination, high light intensity is needed to drive water splitting. In other words, appropriate surface modifications that suppress these back electron transfer reactions are necessary for light-driven water splitting with a dye-sensitized nanosheet photocatalyst.

The apparent quantum yield (AQY), another important metrics in heterogeneous photocatalysis, was also determined. The optimized system gave a maximum AQY of 4.1% at 420 nm (see table S1), again with stoichiometric H_2 and O_2 evolution (fig. S7). This value is the highest among Z-scheme overall water splitting systems that incorporate a dye-sensitized H_2 evolution photocatalyst. Although an approach by "photocatalyst sheet" has recently been shown to substantially improve the Z-scheme activity (*23*, *24*), AQYs recorded in powder suspension systems under visible light still remain several percentages (*19*, *23*, *25*–*27*), and ~10% at the highest (*28*). Considering these, the AQY obtained in this work is comparable to those achieved in conventional semiconductor-based photocatalysts and demonstrates the great potential of a dye-sensitized photocatalyst as a component of Z-scheme overall water splitting.

DISCUSSION

We have successfully improved the efficiency of a Z-scheme overall water splitting system by using a surface-modified dye-sensitized nanosheet photocatalyst. The optimal systems gave an STH conversion efficiency of 0.12% and an AQY of 4.1% at 420 nm, which are new benchmarks for Z-scheme water splitting using dye-sensitized photocatalysts.

The present study highlights that surface modification of dye-sensitized oxide photocatalysts is critically important in terms of suppressing the two principal pathways of back electron transfer reactions, the negative impact of which is most pronounced under irradiation at low intensity. This idea has not been fully appreciated in earlier studies, most of which have been carried out in sacrificial systems (*29*, *30*), in which the negative impact of back electron transfer reactions can be minimized. Understanding the mechanisms of back electron transfer reactions in the hydrogen-evolving component of a Z-scheme enables it to be used more effectively. For example, the STH may be further improved by revisiting dye molecules and H_2-evolving cocatalysts. These findings may also provide a useful guide for the construction of other dye-sensitized systems, such as those that carry out CO_2 reduction (*31*–*33*), because the control of back electron transfer reactions is essential to achieving high efficiency in any nonsacrificial artificial photosynthetic schemes.

MATERIALS AND METHODS

Synthesis of $Ca_2Nb_3O_{10}^-$ nanosheets

First, layered $KCa_2Nb_3O_{10}$ was synthesized by a flux method (*34*). K_2SO_4 (≥99.0%; Kanto Chemical Co.), $CaCO_3$ (≥99.99%; Kanto Chemical Co.), and Nb_2O_5 (≥99.95%; Kanto Chemical Co.) were mixed in a molar ratio of K/Ca/Nb = 5/2/3 using an agate mortar and a pestle. The mixture was put into a Pt crucible and heated at a ramp rate of 300 K $hour^{-1}$ to 1173 K, then at 100 K $hour^{-1}$ to 1573 K, and kept at that temperature for 24 hours. It was cooled down to 1073 K at 25 K $hour^{-1}$ and then naturally cooled. The

obtained sample was centrifuged and washed with water and dried at 343 K overnight.

The as-synthesized $KCa_2Nb_3O_{10}$ was stirred in an aqueous 1 M HNO_3 solution for 3 days. The acid solution was refreshed once on the second day. The product was centrifuged and washed with H_2O thoroughly until the pH of the supernatant became six to seven, followed by drying at 343 K overnight. The prepared $HCa_2Nb_3O_{10}$ was stirred in an aqueous TBA^+OH^- solution [40 weight % (wt %) in H_2O; Sigma Aldrich] for 1 week to obtain $TBA^+/Ca_2Nb_3O_{10}^-$ nanosheets (*35*). The molar ratio of TBA^+ to the exchangeable cations in the protonated solids was 1. The unreacted lamellar solid was removed by decantation. The concentration of the as-prepared $Ca_2Nb_3O_{10}^-$ nanosheet suspension was typically ~5 g liter^{-1}.

Intercalation of Pt nanoparticles into $HCa_2Nb_3O_{10}$ nanosheets

Pt was selectively deposited in the interlayer according to a previous report (*15*). A 1 mM aqueous solution of dissolved $[Pt(NH_3)_4]Cl_2$ (Wako Pure Chemicals) was dropped at a rate of 1 to 2 ml min^{-1} into the as-prepared $Ca_2Nb_3O_{10}^-$ nanosheet suspension (1 wt % Pt), and the suspension was stirred for 1 day. Then, the colloidal nanosheets were restacked by adding an aqueous 2 M HCl solution. The precipitate was washed with H_2O and dried at 343 K. The sample was ground and heated at 473 K for 1 hour under H_2 flow of 20 ml min^{-1}. Last, the product was stirred in aqua regia at the boiling temperature for 15 min to dissolve Pt on the external surface of $HCa_2Nb_3O_{10}$. The bulk amount of Pt loaded was 0.3 to 0.4 wt %, corresponding to a near-surface Pt/Nb atomic ratio of 0.007 to 0.008 from previous XPS measurements (*10*). The restacked Pt/$HCa_2Nb_3O_{10}$ nanosheets had a Brunauer-Emmett-Teller (BET) surface area of 38 m^2 g^{-1}.

Al_2O_3 modification

Al_2O_3 was deposited by a sol-gel method on the as-prepared Pt/$HCa_2Nb_3O_{10}$ (*10*). Pt/$HCa_2Nb_3O_{10}$ (100 mg) was suspended in 20 ml of ethanol containing 100 μl of aqueous 0.1 M H_2SO_4 solution and aluminum isopropoxide (2 wt %, ≥98.0%, TCI). The suspension was subjected to sonication for 30 min, followed by stirring for 1 day. The resulting powder was washed with water and dried at room temperature under a vacuum. The surface Al/Nb atomic ratio in the Al_2O_3-modified Pt/$HCa_2Nb_3O_{10}$ was measured to be 0.2 by XPS (fig. S2B).

Synthesis and adsorption of a Ru(II) photosensitizer

$[Ru(4,4'\text{-}(CH_3)_2\text{-bpy})_2(4,4'\text{-}(PO_3H_2)_2\text{-bpy})]Cl_2$, referred to as **Ru**, was synthesized by literature methods with some modifications (*36*). The successful synthesis of **Ru** was confirmed by ^{1}H nuclear magnetic resonance spectroscopy, electrospray ionization–mass spectroscopy, and ultraviolet-visible (UV-vis) absorption spectroscopy. The spectroscopic and electrochemical properties of **Ru** can be found in our previous paper (*11*). Adsorption of **Ru** onto the nanosheet surface was performed as follows: 50 mg of nanosheet powder was suspended in an appropriate volume of the aqueous Ru(II) complex solution (50 μM). The pH was adjusted to 2 by addition of an aqueous HCl solution. The suspension was stirred for 15 hours at room temperature in the dark, followed by filtration, washing with H_2O, and drying at room temperature under vacuum. The amount of Ru(II) complex adsorbed was estimated from the difference in the ^{1}MLCT absorbance in the UV-vis absorption spectrum before and after adsorption using molar extinction coefficients of Ru(II) complexes reported previously.

PSS modification

PSS modification onto **Ru** adsorbed nanosheets was performed as follows: 50 mg of the **Ru**-adsorbed nanosheet sample was suspended in 20 ml of 0.25 mM poly(sodium 4-styrenesulfonate) (PSS; Sigma-Aldrich, MW 70,000) aqueous solution at pH 2 for 1 hour in the dark, followed by filtration, washing with H_2O, and drying at room temperature under vacuum (*8*).

Transient absorption measurements

Transient absorption spectroscopy measurements were performed using an enVISion transient absorption system (Magnitude Instruments, State College, PA) described previously (*10*, *11*). Briefly, approximately 10 mg of the **Ru**-sensitized $HCa_2Nb_3O_{10}$ nanosheet sample was dispersed in an aqueous NaI (10 or 100 mM, 4 ml, ≥99.9%; Fisher Science Education) or pure water in a quartz cuvette, and spectra were recorded in diffuse reflectance mode. The pH of the solution was adjusted to about 4 with aqueous H_2SO_4 solution. The suspension was purged with Ar at least for 30 min before experiments.

Characterization

Scanning electron microscopy (SEM) images were taken using a Hitachi SU9000 field emission SEM. XPS measurements were conducted using an ESCA-3400 apparatus (Shimadzu). The binding energies were determined by referencing the C 1s peak (284.5 eV) for each sample. UV-vis diffuse reflectance spectra were obtained using a spectrophotometer (V-670, JASCO). The BET surface area was measured using a gas adsorption apparatus (MICROTRAC MRB, BELSORP-mini) at liquid nitrogen temperature (77 K).

Photocatalytic reactions

The experimental detail of photocatalytic reactions was essentially the same as reported previously (*10*). Briefly, 20 mg of dye-adsorbed sample was suspended in an aqueous 100-ml solution containing an electron donor. NaI (≥99.5%), purchased from Kanto Chemical Co. was used as an electron donor without further purification. The pH of the reaction solution was adjusted to 4 with aqueous HCl solution. When Z-scheme overall water splitting was performed, 50 mg of PtO_x/H-Cs-WO_3 photocatalyst (*18*, *37*) was used together with the dye-adsorbed H_2 evolution photocatalyst. The details of the preparation and characterization of the O_2 evolution photocatalyst can be found in a previous paper (*18*). Our previous study has shown that the optimal pH of the solution for nonsacrificial overall water splitting in the presence of NaI is ~4 (*10*). The light source was a 300-W xenon lamp (Cermax, PE300BF) fitted with a CM-1 cold mirror and an L42 cutoff filter to allow for visible light irradiation ($\lambda > 400$ nm). The irradiation area was 44 cm^2. The light intensity was measured using a calibrated silicon photodiode to be 80 mW cm^{-2} in the wavelength range of 400 to 600 nm. For experiments with lower-intensity visible light (8.0 mW cm^{-2}), a neutral density filter was used. These photoreaction experiments were conducted at room temperature using a top irradiation–type cell connected to a closed gas circulation system made of glass. The evolved gases were analyzed by gas chromatography (Shimadzu, GC-8A with a TCD detector and an MS-5A column, argon carrier gas).

STH conversion efficiency was measured using a HAL-320 solar simulator as the light source and was estimated according to the following equation

$$\mathrm{STH}\ (\%) = \frac{R_H \times \Delta G^{\circ}}{P \times S} \times 100 = \frac{2R_O \times \Delta G^{\circ}}{P \times S} \times 100 \quad (6)$$

where R_H, R_o, ΔG^o, P, and S are the rates of hydrogen/oxygen evolution (mol s^{-1}) in Z-scheme water splitting, the standard Gibbs free energy of liquid water (237×10^3 J mol^{-1}), the intensity of simulated sunlight (50, 100, or 200 mW cm^{-2}), and the irradiation area (9 cm^2).

The AQY for H_2 evolution was measured using a band-pass filter (λ = 420 nm) and was estimated as

$$\mathrm{AQY}(\%) = \frac{A \times R}{I} \times 100 \quad (7)$$

where A, R, and I represent the reaction coefficient (H_2 evolution, 4; O_2 evolution, 8), the H_2 or O_2 evolution rate, and the rate of incident photons, respectively (*18*, *25*). The rate of incident photons (1.03 mW cm^{-2}) was measured using a calibrated silicon photodiode. The irradiation area was 44 cm^2. In the AQY measurements, the amounts of photocatalysts used were changed for optimization of the performance (*25*).

SUPPLEMENTARY MATERIALS

Supplementary material for this article is available at https://science.org/doi/10.1126/sciadv.adc9115

View/request a protocol for this paper from *Bio-protocol*.

REFERENCES AND NOTES

1. K. Maeda, K. Domen, Photocatalytic water splitting: Recent progress and future challenges. *J. Phys. Chem. Lett.* **1**, 2655–2661 (2010).
2. H. Nishiyama, T. Yamada, M. Nakabayashi, Y. Maehara, M. Yamaguchi, Y. Kuromiya, Y. Nagatsuma, H. Tokudome, S. Akiyama, T. Watanabe, R. Narushima, S. Okunaka, N. Shibata, T. Takata, T. Hisatomi, K. Domen, Photocatalytic solar hydrogen production from water on a 100-m^2 scale. *Nature* **598**, 304–307 (2021).
3. W. J. Youngblood, S.-H. A. Lee, K. Maeda, T. E. Mallouk, Visible light water splitting using dye-sensitized oxide semiconductors. *Acc. Chem. Res.* **42**, 1966–1973 (2009).
4. R. Abe, Development of a new system for photocatalytic water splitting into H_2 and O_2 under visible light irradiation. *Bull. Chem. Soc. Jpn.* **84**, 1000–1030 (2011).
5. A. Nakada, H. Kumagai, M. Robert, O. Ishitani, K. Maeda, Molecule/semiconductor hybrid materials for visible-light CO_2 reduction: Design principles and interfacial engineering. *Acc. Mater. Res.* **2**, 458–470 (2021).
6. F. E. Osterloh, Photocatalysis versus photosynthesis: A sensitivity analysis of devices for solar energy conversion and chemical transformations. *ACS Energy Lett.* **2**, 445–453 (2017).
7. Y. I. Kim, S. J. Atherton, E. S. Brigham, T. E. Mallouk, Sensitized layered metal oxide semiconductor particles for photochemical hydrogen evolution from nonsacrificial electron donors. *J. Phys. Chem.* **97**, 11802–11810 (1993).
8. G. B. Saupe, T. E. Mallouk, W. Kim, R. H. Schmehl, Visible light photolysis of hydrogen iodide using sensitized layered metal oxide semiconductors: The role of surface chemical modification in controlling back electron transfer reactions. *J. Phys. Chem. B* **101**, 2508–2513 (1997).
9. R. Abe, K. Shinmei, N. Koumura, K. Hara, B. Ohtani, Visible-light-induced water splitting based on two-step photoexcitation between dye-sensitized layered niobate and tungsten oxide photocatalysts in the presence of a triiodide/iodide shuttle redox mediator. *J. Am. Chem. Soc.* **135**, 16872–16884 (2013).
10. T. Oshima, S. Nishioka, Y. Kikuchi, S. Hirai, K. I. Yanagisawa, M. Eguchi, Y. Miseki, T. Yokoi, T. Yui, K. Kimoto, K. Sayama, O. Ishitani, T. E. Mallouk, K. Maeda, An artificial Z-scheme constructed from dye-sensitized metal oxide nanosheets for visible light-driven overall water splitting. *J. Am. Chem. Soc.* **142**, 8412–8420 (2020).
11. S. Nishioka, T. Oshima, S. Hirai, D. Saito, K. Hojo, T. E. Mallouk, K. Maeda, Excited carrier dynamics in a dye-sensitized niobate nanosheet photocatalyst for visible-light hydrogen evolution. *ACS Catal.* **11**, 659–669 (2021).
12. K. Hojo, S. Nishioka, Y. Miseki, Y. Kamakura, T. Oshima, K. Sayama, T. E. Mallouk, K. Maeda, An improved Z-scheme for overall water splitting using dye-sensitized calcium niobate nanosheets synthesized by a flux method. *ACS Appl. Energy Mater.* **4**, 10145–10152 (2021).
13. F. E. Osterloh, Inorganic nanostructures for photoelectrochemical and photocatalytic water splitting. *Chem. Soc. Rev.* **42**, 2294–2320 (2013).
14. K. Maeda, T. E. Mallouk, Two-dimensional metal oxide nanosheets as building blocks for artificial photosynthetic assemblies. *Bull. Chem. Soc. Jpn.* **92**, 38–54 (2019).
15. T. Oshima, D. Lu, O. Ishitani, K. Maeda, Intercalation of highly dispersed metal nanoclusters into a layered metal oxide for photocatalytic overall water splitting. *Angew. Chem. Int. Ed.* **54**, 2698–2702 (2015).
16. T. P. Nguyen, S. A. de Vos, An investigation into the effect of chemical and thermal treatments on the structural changes of poly(3,4-ethylenedioxythiophene)/polystyrenesulfonate and consequences on its use on indium tin oxide substrates. *Appl. Surf. Sci.* **221**, 330–339 (2004).
17. W. Kim, T. Tachikawa, T. Majima, W. Choi, Photocatalysis of dye-sensitized TiO_2 nanoparticles with thin overcoat of Al_2O_3: Enhanced activity for H_2 production and dechlorination of CCl_4. *J. Phys. Chem. C* **113**, 10603–10609 (2009).
18. Y. Miseki, S. Fujiyoshi, T. Gunji, K. Sayama, Photocatalytic water splitting under visible light utilizing I_3^-/I^- and IO_3^-/I^- redox mediators by Z-scheme system using surface treated PtO_x/WO_3 as O_2 evolution photocatalyst. *Cat. Sci. Technol.* **3**, 1750 (2013).
19. H. Kato, Y. Sasaki, N. Shirakura, A. Kudo, Synthesis of highly active rhodium-doped $SrTiO_3$ powders in Z-scheme systems for visible-light-driven photocatalytic overall water splitting. *J. Mater. Chem. A* **1**, 12327–12333 (2013).
20. K. Maeda, K. Domen, Development of novel photocatalyst and cocatalyst materials for water splitting under visible light. *Bull. Chem. Soc. Jpn.* **89**, 627–648 (2016).
21. T. Hisatomi, K. Maeda, K. Takanabe, J. Kubota, K. Domen, Aspects of the water splitting mechanism on $(Ga_{1-x}Zn_x)(N_{1-x}O_x)$ photocatalyst modified with $Rh_{2-y}Cr_yO_3$ cocatalyst. *J. Phys. Chem. C* **113**, 21458–21466 (2009).
22. R. Han, M. A. Melo, Z. Zhao, Z. Wu, F. E. Osterloh, Light intensity dependence of photochemical charge separation in the $BiVO_4$/Ru-$SrTiO_3$:Rh direct contact tandem photocatalyst for overall water splitting. *J. Phys. Chem. C* **124**, 9724–9733 (2020).
23. Q. Wang, Y. Li, T. Hisatomi, M. Nakabayashi, N. Shibata, J. Kubota, K. Domen, Z-scheme water splitting using particulate semiconductors immobilized onto metal layers for efficient electron relay. *J. Catal.* **328**, 308–315 (2015).
24. Q. Wang, T. Hisatomi, Q. Jia, H. Tokudome, M. Zhong, C. Wang, Z. Pan, T. Takata, M. Nakabayashi, N. Shibata, Y. Li, I. D. Sharp, A. Kudo, T. Yamada, K. Domen, Scalable water splitting on particulate photocatalyst sheets with a solar-to-hydrogen energy conversion efficiency exceeding 1. *Nat. Mater.* **15**, 611–615 (2016).
25. K. Maeda, M. Higashi, D. Lu, R. Abe, K. Domen, Efficient nonsacrificial water splitting through two-step photoexcitation by visible light using a modified oxynitride as a hydrogen evolution photocatalyst. *J. Am. Chem. Soc.* **132**, 5858–5868 (2010).
26. S. Chen, Y. Qi, T. Hisatomi, Q. Ding, T. Asai, Z. Li, S. S. Ma, F. Zhang, K. Domen, C. Li, Efficient visible-light-driven Z-scheme overall water splitting using a $MgTa_2O_{6-x}N_y$/TaON heterostructure photocatalyst for H_2 evolution. *Angew. Chem. Int. Ed.* **54**, 8498–8501 (2015).
27. K. Ogawa, A. Nakada, H. Suzuki, O. Tomita, M. Higashi, A. Saeki, H. Kageyama, R. Abe, Flux synthesis of layered oxyhalide Bi_4NbO_8Cl photocatalyst for efficient Z-scheme water splitting under visible light. *ACS Appl. Mater. Interfaces* **11**, 5642–5650 (2019).
28. Y. Qi, Y. Zhao, Y. Gao, D. Li, Z. Li, F. Zhang, C. Li, Redox-based visible-light-driven Z-scheme overall water splitting with apparent quantum efficiency exceeding 10%. *Joule* **2**, 2393–2402 (2018).
29. P. Chowdhury, G. Malekshoar, A. Ray, Dye-sensitized photocatalytic water splitting and sacrificial hydrogen generation: Current status and future prospects. *Inorganics* **5**, 34 (2017).
30. M. Watanabe, Dye-sensitized photocatalyst for effective water splitting catalyst. *Sci. Technol. Adv. Mater.* **18**, 705–723 (2017).
31. T. W. Woolerton, S. Sheard, E. Reisner, E. Pierce, S. W. Ragsdale, F. A. Armstrong, Efficient and clean photoreduction of CO_2 to CO by enzyme-modified TiO_2 nanoparticles using visible light. *J. Am. Chem. Soc.* **132**, 2132–2133 (2010).
32. D. I. Won, J. S. Lee, J. M. Ji, W. J. Jung, H. J. Son, C. Pac, S. O. Kang, Highly robust hybrid photocatalyst for carbon dioxide reduction: Tuning and optimization of catalytic activities of Dye/TiO_2/Re(I) organic-inorganic ternary systems. *J. Am. Chem. Soc.* **137**, 13679–13690 (2015).
33. M. Abdellah, A. M. El-Zohry, L. J. Antila, C. D. Windle, E. Reisner, L. Hammarstrom, Time-resolved IR spectroscopy reveals a mechanism with TiO_2 as a reversible electron acceptor in a TiO_2-Re catalyst system for CO_2 photoreduction. *J. Am. Chem. Soc.* **139**, 1226–1232 (2017).
34. Y. Song, N. Iyi, T. Hoshide, T. C. Ozawa, Y. Ebina, R. Ma, N. Miyamoto, T. Sasaki, Accordion-like swelling of layered perovskite crystals via massive permeation of aqueous solutions into 2D oxide galleries. *Chem. Commun.* **51**, 17068–17071 (2015).
35. Y. Ebina, N. Sakai, T. Sasaki, Photocatalyst of lamellar aggregates of RuO_x-loaded perovskite nanosheets for overall water splitting. *J. Phys. Chem. B* **109**, 17212–17216 (2005).
36. D. L. Ashford, M. K. Brennaman, R. J. Brown, S. Keinan, J. J. Concepcion, J. M. Papanikolas, J. L. Templeton, T. J. Meyer, Varying the electronic structure of surface-bound ruthenium(II) polypyridyl complexes. *Inorg. Chem.* **54**, 460–469 (2015).

37. Y. Miseki, K. Sayama, Photocatalytic water splitting employing a $[Fe(CN)_6]^{3-/4-}$ redox mediator under visible light. *Cat. Sci. Technol.* **9**, 2019–2024 (2019).

Acknowledgments
Funding: This work was supported by a Grant-in-Aid for Scientific Research (B) (JP19H02511 and JP22H01862), a Grant-in-Aid for Transformative Research Areas (A) "Supra-ceramics" (JP22H05148) (JSPS), and the Mazda Foundation. S.N. wishes to acknowledge support by a Grant-in-Aid for Research Activity Start-up (JP21K20555). T.E.M. acknowledges support from the Office of Basic Energy Sciences, Division of Chemical Sciences, Geosciences, and Energy Biosciences, Department of Energy, under contract DE-SC0019781. K.M. wishes to thank the ENEOS Hydrogen Trust Fund and the Japan Science and Technology Agency (JST) CREST program (JPMJCR20R2). **Author contributions:** Conceptualization: T.E.M. and K.M. Investigation: S.N., K.H., L.X., T.G., Y.M., S.Y., T.Y., and K.S. Supervision: K.M. Writing—original draft: S.N. and K.H. Writing—review and editing: T.E.M. and K.M. **Competing interests:** The authors declare that they have no competing interests. **Data and materials availability:** All data needed to evaluate the conclusions in the paper are present in the paper and/or the Supplementary Materials.

Submitted 9 May 2022
Accepted 29 June 2022
Published 10 August 2022
10.1126/sciadv.adc9115